

REVIEW

Advances in MRI-guided precision radiotherapy

Chenyang Liu¹ | Mao Li² | Haonan Xiao¹ | Tian Li¹ | Wen Li¹ | Jiang Zhang¹ |
Xinzhi Teng¹ | Jing Cai¹ 

¹ Department of Health Technology and Informatics, The Hong Kong Polytechnic University, Hong Kong SAR, China

² Department of Radiation Oncology, Philips Healthcare, Chengdu, China

Correspondence

Jing Cai, PhD, Department of Health Technology and Informatics, The Hong Kong Polytechnic University, Hong Kong, China.
Email: jing.cai@polyu.edu.hk

Chenyang Liu and Mao Li contributed equally to the manuscript.

Funding information

General Research Fund, Grant/Award Numbers: 15102118, 15102219; University Grants Committee, Health and Medical Research Fund, Grant/Award Number: 06173276; Food and Health Bureau; Innovation and Technology Fund, Grant/Award Number: ITS/080/19; Innovation and Technology Commission; Government of the Hong Kong Special Administrative Region

Abstract

Magnetic resonance imaging (MRI) is becoming increasingly important in precision radiotherapy owing to its excellent soft-tissue contrast and versatile scan options. Many recent advances in MRI have been shown to be promising for MRI-guided radiotherapy and for improved treatment outcomes. This paper summarizes these advances into six sections: MRI simulators, MRI-linear accelerator hybrid machines, MRI-only workflow, four-dimensional MRI, MRI-based radiomics, and magnetic resonance fingerprinting. These techniques can be implemented before, during, or after radiotherapy for various precision radiotherapy applications, such as tumor delineation, tumor motion management, treatment adaptation, and clinical decision making. For each of these techniques, this paper describes its technical details and discusses its clinical benefits and challenges.

KEYWORDS

4D-MRI, MR-Linac, MRI-guided radiotherapy

1 | INTRODUCTION

Cancer is the main lethal disease for humans in the 21st century. Radiotherapy, as one of the most conventional methods for cancer treatment, participates in approximately 50% of cancer treatments and cures 40% of cancer patients.¹ Recently, precision radiotherapy has received considerable attention under the trend of precision medicine.² The utilization of imaging modalities (e.g., computed tomography [CT], magnetic resonance imaging [MRI], and ultrasound) before, during, and after radiation delivery, namely, image-guided radiotherapy (IGRT), has greatly improved the precision and accuracy of radiotherapy.³ These imaging modalities are used in almost all steps of radiotherapy, including pretreatment simulation and position,

treatment planning, treatment adaption, online monitoring, and post-treatment follow-up and evaluation. Traditional IGRT focuses on CT-guided radiotherapy because CT has (1) fast image acquisition speed, (2) inherent electron density information for dose calculation, (3) no spatial distortion within the effective field-of-view (FOV), and (4) digitally reconstructed radiograph (DRR) for position verification.⁴ However, the intrinsic low soft-tissue contrast of CT images cannot fulfill the increasingly stringent requirement of precision radiotherapy.

MRI presents superior soft-tissue contrast to other imaging modalities. The proportion of MRI-guided radiotherapy has increased rapidly in the past few years.⁵ The high soft-tissue contrast in MRI images enables a clearer boundary between the tumor and surrounding structures, which improves the delineation accuracy of treatment target

This is an open access article under the terms of the [Creative Commons Attribution-NonCommercial-NoDerivs](https://creativecommons.org/licenses/by-nc-nd/4.0/) License, which permits use and distribution in any medium, provided the original work is properly cited, the use is non-commercial and no modifications or adaptations are made.

© 2022 The Authors. *Precision Radiation Oncology* published by John Wiley & Sons Australia, Ltd on behalf of Shandong Cancer Hospital & Institute.

areas and organs at risk (OARs). Apart from high soft-tissue contrast, the trend of MRI-guided radiotherapy stems from several further advantages of MRI over other imaging modalities, including (1) ionizing radiation-free imaging that eliminates the image dose concern for multiple MRI scans during radiotherapy; (2) versatile imaging sequences that provide multi-parameter and multi-contrast information; (3) no imaging plane restriction; and (4) functional MRI and quantitative MRI techniques that provide biological characteristics of the tumor and surrounding tissues. Despite these benefits, the application of MRI-guided radiotherapy encounters many challenges. One challenge is the relatively long MRI time, especially when compared with time-efficient CT scans. The scan time of multi-parametric or functional MRI could take 30 min or even 1 h, which is intolerable for some patients with poor physical conditions. The difficulty in dose calculation is also an important consideration in MRI-guided radiotherapy. A pretreatment CT scan is essential to obtain electron density information for dose calculation. In addition, the MR images are subjective to geometric distortion, especially in the case of the large FOV MRI scan. The geometric distortion will consequently decrease the accuracy of radiation dose delivery. In terms of clinical challenges, MRI-guided radiotherapy lacks standardized clinical protocols and suitable devices.⁶ MRI quality assurance (QA) for diagnoses and radiotherapy follows different criteria and utilizes different specialized phantoms. However, there are no standardized QA protocols for MRI-guided radiation therapy. Also, few magnetic resonance devices are dedicated to MRI-guided radiotherapy. For example, conventional MRI receiver coils are not suitable for MRI simulators.

Recent technological developments in MRI hardware and software have largely resolved the above-mentioned challenges in MRI-guided radiotherapy. MRI scanners customized for radiotherapy simulation have been applied to the clinic. The magnetic resonance-Linac (MR-Linac) machine has achieved direct treatment implementation after rapid scanning, which makes it possible to monitor the movement of the target area during the treatment process. At the same time, advanced MRI protocols present an extra time dimension for evaluating the position changes of the treatment target volume and its surrounding normal tissues. MRI-guided radiotherapy also benefits from the rapid development of artificial intelligence and data sciences.⁷ Hence, it is desirable to review recent technical advances in the field of MRI-guided radiotherapy that contribute to precision radiotherapy. This review paper surveyed recent published peer-review papers that are related to MRI-guided radiotherapy and summarizes them into six sections, which have been structured in ascending order of the application distance from current clinical practice: Section 2 introduces MRI simulation, which was emphasized in the current clinical procedure; Section 3 summarizes MR-Linac; Section 4 describes the MRI-only workflow with a focus on image synthesis; Section 5 introduces four-dimensional MRI (4D-MRI), which adds an extra time dimension for improved motion management; Section 6 presents MRI-based radiomics modeling techniques used for decision-making; and Section 7 highlights the potential application direction of the novel quantitative magnetic resonance fingerprinting techniques. The conclusions are drawn in Section 8.

2 | MRI SIMULATION

The purpose of the simulation scan is to localize the treatment site, delineate tumor target volume and OARs, and perform radiation treatment planning. Currently, MRI simulation is the main clinical practice in MRI-guided radiotherapy, and has been applied to both external beam radiotherapy and brachytherapy.^{8,9}

At the ASTRO conference in 1993, Okamoto presented the prototype MRI positioning system in a 1.5 T MRI.¹⁰ Restricted by the hardware of superconducting magnets, early-stage MRI simulators have a relatively small bore size of 60 cm. Large-size body position fixation devices (e.g., vacuum pads, polyurethane foam casts, and thermoplastic fixation masks) are difficult to accommodate in MRI simulators. Unlike CT, which can have a large bore size of 85 cm or even 90 cm, increasing the bore size of MRI is challenging. Increasing the bore size requires more coils, which increases the weight of the MRI scanner. More importantly, increasing the bore size will challenge the magnetic homogeneity, which is an important indicator to ensure image quality, fat suppression, and image distortion. Alternatively, a low-field open MRI system was developed for simulation scanning to avoid bore size restriction.¹¹ However, the relatively low field strength in an open MRI system sacrifices the image quality, prolongs the scan time, and abandons the functional scan. With the development of MRI hardware, high-field, wide-bore MRI has become the mainstream. The bore size of MRI can reach 70 cm, which meets the positioning space requirements of the radiotherapy.¹² Currently, MRI scanners customized for radiotherapy simulation have been applied in the clinic (Figure 1), and feature the following characteristics:

1. Bore size ≥ 70 cm.
2. External 3D laser light positioning system.
3. Flat treatment bed dedicated for radiotherapy.
4. Receiver coil bridge dedicated for radiotherapy.
5. Scanning sequence dedicated to radiotherapy positioning.
6. MRI QA phantom and QA program dedicated to radiotherapy.

The MRI scanning sequence protocols for simulation are different from diagnosis to meet the simulation-specific criteria. Table 1 summarizes the difference between sequences used for diagnoses and simulation planning. Fast spin-echo (FSE), as known as turbo spin-echo (TSE), T1/T2-weighted imaging is the main scan sequence used for MRI simulation. Three-dimensional (3D) sequences are mostly used in MRI simulation for the reason of no slice selection requirement and minimum edge distortion between image slices. In addition to FSE/TSE, gradient echo sequence T1/T2-weighted imaging is applied to MRI simulation for enhancement scanning.

MRI simulation can be applied to various tumor regions, even to regions where MRI is rarely employed for diagnoses.¹³ For example, the delineation of the target volume of lung tumors has benefited from MRI simulation even though MRI is rarely used in lung cancer diagnosis.¹⁴ Using a simulation CT scan to delineate the target volume is challenging due to the poor contrast of the soft tissue of CT images. Lung cancer, obstructive pneumonia, and atelectasis cannot be



FIGURE 1 MRI simulation systems

TABLE 1 The difference between sequences used for diagnoses and simulation planning

	MRI for diagnosis	MRI for radiotherapy treatment planning
Scanning plane	Angulated to anatomy	Orthogonal transverse plane without slice angulation
Spatial accuracy	Less important	Geometrical fidelity is important
FOV	Depending on the anatomy	Large FOV and large coverage
Geometric correction	Not necessary	Requirement
Bandwidth	Low readout bandwidth for high SNR	High readout bandwidth for less WFS
Scan dimension	Mostly use 2D sequences and have slice gap	Mostly use 3D sequences, zero-gap
Slices thickness	Thick slices for high SNR	Thin slices for high resolution in all dimensions, sometimes isotropic

Abbreviations: MRI, magnetic resonance imaging; FOV, field of view; SNR, Singal-Noise Ratio; WFS, Water Fat Shift.

distinguished on the CT image, for example, as both the tumor region and the area of obstructive atelectasis showed enhancement in the image. In contrast, MRI simulation could use contrast enhancement or functional MRI scans to identify atelectasis, diagnose the mediastinum, and assess the recurrence of lung cancer.¹⁵ Figure 2 presents an example of using apparent diffusion coefficient (ADC) maps to distinguish between distal atelectasis tissue and lung cancer tissue.

3 | MR-LINAC

MR-Linac is one of the largest technological advances in MRI-guided radiotherapy. It integrates a magnetic resonance scanner with a linear

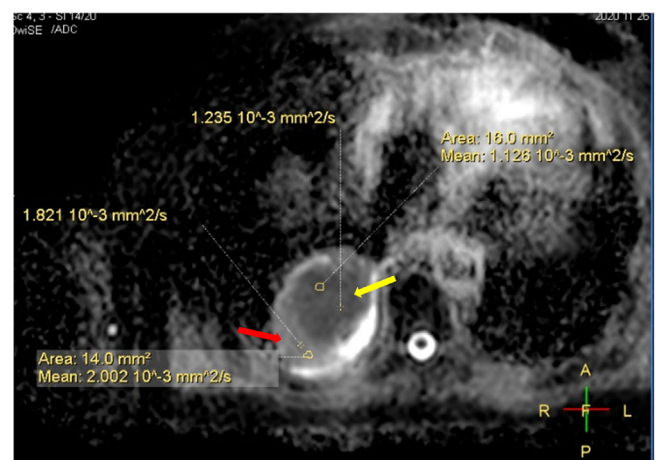


FIGURE 2 ADC maps to distinguish between distal atelectasis tissue (red arrow) and lung cancer tissue (yellow arrow)

TABLE 2 Commercially available MRI-Linac systems

Institution	B_0 field (T)	Magnet type	Beam-field orientation
ViewRay/MRIdian	0.35	Open	Perpendicular
Alberta/Magnet Tx	0.5	Open	Inline and perpendicular
Australia MR-Linac	1.0	Open	Inline and perpendicular
Elekta/Unity MR-Linac	1.5	Closed	Perpendicular

accelerator. The Cancer Institute of the University of Alberta in Canada developed the first MR-Linac. Since then, major research institutes and manufacturers have developed various types of MR-Linac systems.¹⁶ Table 2 lists the commercially available MR-Linac systems.

3.1 | The hardware of MR-Linac

Due to conflicts in the design principles between magnetic resonance and linear accelerators, integrating these two components has several technical challenges, especially under high magnetic field strength

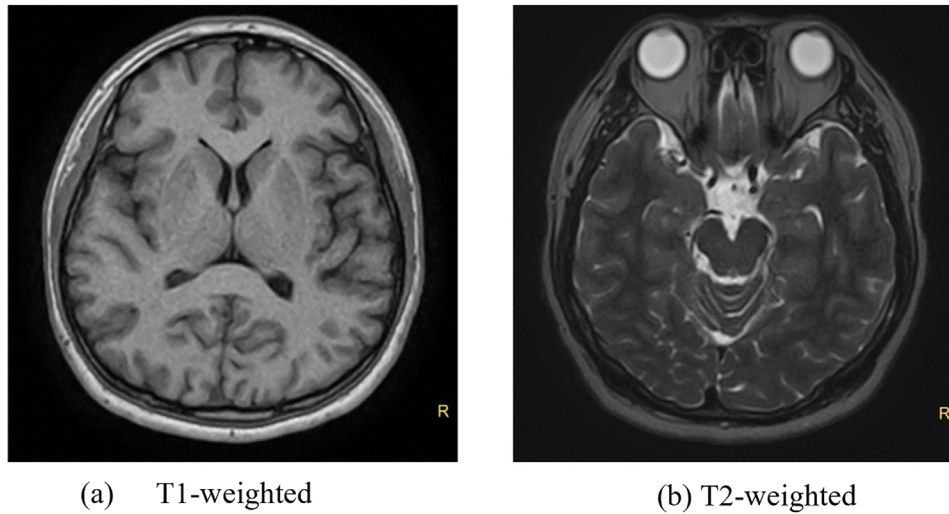


FIGURE 3 Brain MRI images acquired on a 1.5 T MR-Linac unity, including (A) T1-weighted MRI image and (B) T2-weighted MRI image

(>1.0 T). However, high-quality MR imaging requires a high signal-to-noise ratio, which is positively correlated with high field strength. In 2018, the first high-field MR-Linac, named Unity, was developed and clinically introduced. It was approved by the Food and Drug Administration (FDA) in December 2018 and treated the first patient in North America at the MD Anderson Cancer Center in January 2019.¹⁷ Unity MR-Linac consists of a 1.5 T magnetic resonance imaging system and a 7-megavolt (7 MV) linear accelerator. A ring gantry holds all the beam-generating components of Linac and is positioned around the cryostat of the MRI. Different from conventional MRI systems, gaps are designed in many magnet resonance components to ensure the passage of megavolt beams, including the main magnetic, gradient coils, and built-in body coils. This discrete hardware introduces magnetic field inhomogeneity and reduces the gradient performance. In terms of image quality, though meeting clinical needs, Unity's image has a slightly lower signal-to-noise ratio than the conventional 1.5 T MR image. Figure 3 demonstrates brain MR images scanned by Unity MR-Linac.

3.2 | Online adaptive radiotherapy

MR-Linac makes it possible for online MRI-guided radiotherapy and adaptive radiotherapy. Previously, IGRT was achieved by a kilovolt-level cone beam CT (CBCT). However, the image quality obtained by CBCT is suboptimal. Unity MR-Linac obtains high-quality MR images before radiotherapy with treatment setup. Thereafter, the position and shape variations of the target volume (gross target volume [GTV] or clinical target volume [CTV]) and OARs can be assessed by comparing against the reference plan. Based on the image information, two treatment modes, adapt to position (ADP) and adapt to shape (ADS), can be chosen to adjust the treatment plan to improve the planning accuracy and reduce the amount of repeated planning.¹⁸ Online adaptive radiotherapy could monitor the intrafraction motion and access the motion

impact on the planned dose distribution. One recent study quantified the delivered dose for prostate patients treated on a Unity MR-Linac based on online 3D cine-MR and treatment log files.¹⁹

The development of fast MR imaging techniques largely reduced the imaging latency. For example, one study achieved a latency time of 300–500 ms in real-time 3D MR imaging on MR-Linac.²⁰ With further reduced latency time in real-time MRI, real-time adaptive treatment is possible in MR-Linac by irradiating moving targets using multileaf collimator (MLC) tracking and real-time dose calculation. Deep learning strategies have been used for real-time dose calculation.²¹ Further evaluation of the accuracy of real-time imaging and dose calculation needs to be implemented in real-time MRI-guided workflows.

4 | MRI-ONLY WORKFLOW

Multi-modality image registration increases the uncertainty in radiotherapy. Many studies have been performed to investigate the feasibility of MRI-only workflow. Treatment planning and dose calculation are performed without the need for a CT simulation scan. CT image synthesis is the main approach to obtain electron density information in MRI-only workflow. Besides CT synthesis, many other synthesis techniques have the potential to be incorporated into MRI-guided radiotherapy. This section also introduces functional MRI (fMRI) synthesis and contrast-enhanced MRI (CE-MRI) synthesis.

4.1 | Synthetic CT technique

A CT simulation scan is required in the MRI simulation workflow to obtain electronic density information. The CT image, as the main image, is used for the dose calculation, and the MR image, as a secondary image, is used to assist the delineation of the target volume. This extra CT scan increases the complexity of MRI-guided

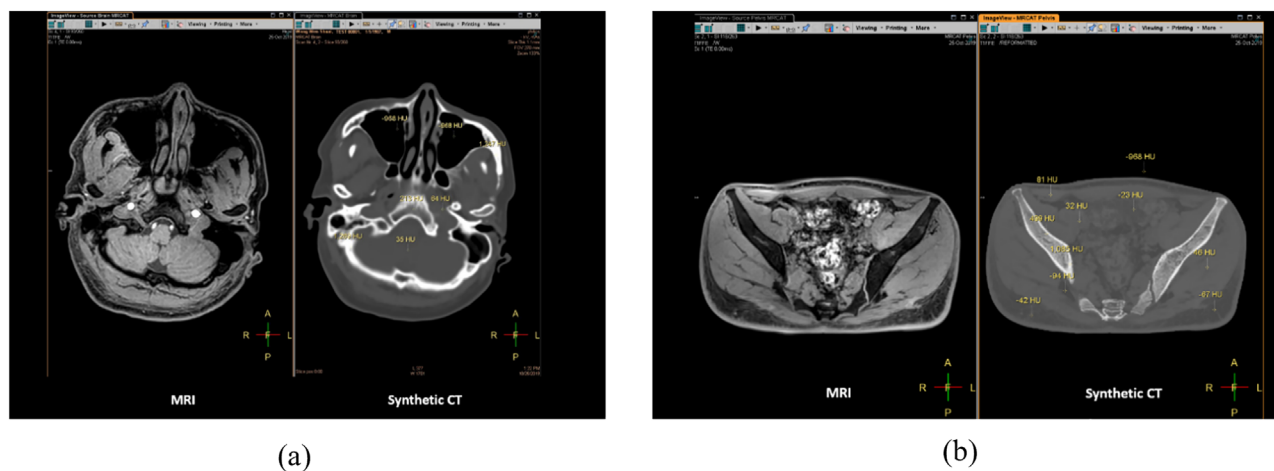


FIGURE 4 sCT technology in (A) brain and (B) the pelvic cavity. The left image is the original MRI image and the right image is the sCT image

radiotherapy. For example, registering CT to MRI introduces geometrical uncertainty. As an alternative, synthetic CT (sCT) image technology has been developed to simulate pseudo-CT images from MRI. The synthesized image contains CT value (Hounsfield unit, HU) information, which can be used directly for dose calculation and patient positioning.^{22,23} Figure 4 presents two examples of sCT. The application of sCT for dose calculation has the potential of replacing CT simulation. It simplifies the MRI simulation workflow by using MRI images for both target area delineation and dose calculation, namely, MRI-only simulation. Current synthetic simulation techniques can be divided into three categories: (1) bulk density sCT techniques; (2) atlas-based sCT techniques; and (3) voxel-based sCT techniques.²⁴ Currently, instead of research institution-driven technique exploration, several companies have developed and commercialized sCT techniques. For example, a commercial software, Magnetic Resonance for Calculation Attenuation (MRCAT), developed by Philips, demonstrated a data consistency of 98% between sCT with reference CT images. The dose distribution maps calculated by sCT images and real CT images have no clear difference.²⁵ However, the application of sCT is restricted to some anatomical regions. A whole-body sCT technique is still not available. More importantly, the consistency between the sCT image and the real CT image needs to be further verified, and safety and ethical issues are still under discussion.²⁶ One study reported the first clinical experience that used MRI-only simulation for treatment planning. A total of 585 patients with prostate cancer were included in this study and underwent an MRI-only simulation. MRI-only simulation was successful in 544 (93.2%) patients and the resting patient underwent a backup CT scan because of the failure of reconstructing the sCT caused by large patient size, artifacts, and motion.⁵

4.2 | Functional MRI synthesis

Historically, fMRI refers to a class of MRI techniques to describe spatial-temporal variation in brain metabolism.²⁷ Now it is generalized

as a set of special MRI scan protocols to provide quantitative information (e.g., perfusion, diffusion) of cancer-related tissue variations.²⁸ fMRI captures cancer-specific characteristics, such as tissue perfusion, oxygenation, and microvessel density. Thereby, fMRI techniques have been integrated with MRI-guided radiotherapy for diagnosis, treatment planning, and treatment response assessment, serving as a powerful tool for personalized radiotherapy. The application of fMRI in MRI-guided radiotherapy has encountered many constraints, such as labor, time, financial cost, and potential hazards. Artificial intelligence may accelerate the application of fMRI by using data-driven fMRI synthesis. For example, diffusion-weighted MRI (DWI) has been widely used for cancer evaluation because of its high sensitivity. However, a high b-value DWI requires a prolonged acquisition time. One study utilized generative adversarial networks (GANs) to synthesize high-b-value diffusion-weighted images for prostate cancer patients.²⁹ The results demonstrated deep learning could synthesize realistic high-b-value DWI with satisfying image quality and accuracy.

4.3 | CE-MRI synthesis

CE-MRI is obtained through the injection of gadolinium-based contrast agents (GBCAs) and is used to improve the clarity of the tumor-to-normal tissue interface for accurate tumor delineation.³⁰ However, nephrogenic systemic fibrosis (NSF), a serious disease that can lead to joint contractures and immobility, has been observed to have a strong connection with the injection of GBCAs in recent studies.^{31,32} For safety considerations, there is an urgent need to eliminate the use of GBCAs. Interests are focused on synthesizing the virtual contrast-enhanced MRI (VCE-MRI) through deep learning to eliminate the use of GBCAs while reserving the enhanced contrast information.^{33–35} The VCE-MRI, which has a similar function to the GBCA-based CE-MRI, is generated from the information provided by contrast-free MRI (Figure 5). The contrast-enhanced region is indicated in the in the red arrow.

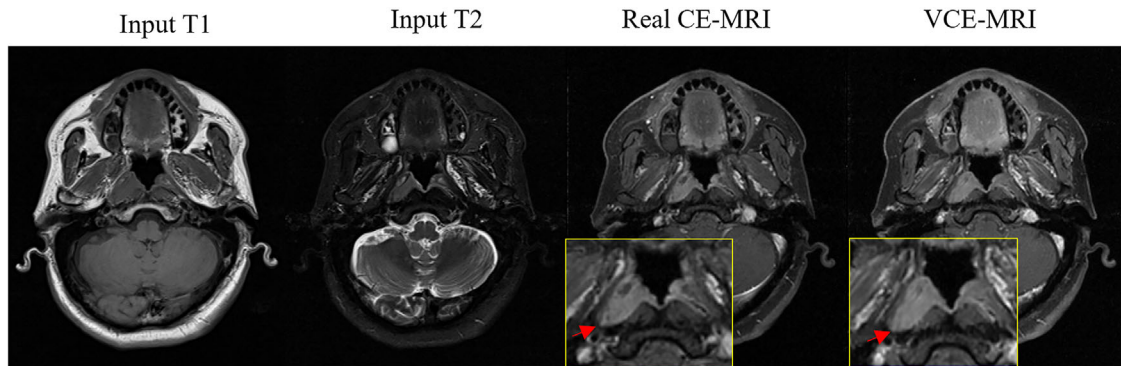


FIGURE 5 Illustration of deep learning-based virtual contrast-enhanced MRI synthesis. The images from left to right are input T1, input T2, real gadolinium-based contrast-enhanced MRI, and the synthetic virtual contrast-enhanced MRI through deep learning

5 | FOUR-DIMENSIONAL-MRI

The 4D medical imaging technique includes a time dimension for the medical image and presents the motion of tumor target and organs-at-risk. Motion information is beneficial to many aspects in radiotherapy, such as determining planning target volume, treatment planning, and tumor position tracking during treatment. For example, dynamic MRI has been used for monitoring real-time lung motion. The probability distribution function (PDF) of patient geometries could be calculated from dynamics MRI and used for treatment planning. PDF-based treatment planning is an off-line strategy that the dose is adjusted by the probability of the organs at a specific location.^{36,37} 4D-CT is the standard option in current radiotherapy for motion management. As an alternative, 4D-MRI has been developed to solve the intrinsic poor soft-tissue contrast problem in 4D-CT. The 4D-MRI technique can be categorized into retrospective and prospective methods.³⁸ Retrospective 4D-MRI continuously acquires images over the entire region of interest (ROI) and retrospectively sorts the images into respiratory phase bins.^{39–41} Retrospective binning is based on different types of breathing surrogates, which are either calculated from medical images (e.g., diaphragm and liver dome position, body area, thermal noise) or extracted from external devices (e.g., breath signal).^{40,42–44} Prospective 4D-MRI methods rely on fast 3D acquisition or respiratory-gated two-dimensional (2D) acquisition.^{45,46} 3D acquisition mainly uses gradient-echo sequences and provides 3D T1-weighted images with a subsecond speed, while respiratory-gated 2D acquisition can monitor the data sufficiency of each phase bin in real time and overcome the data incompleteness problem in retrospective sorting.

Although 4D-MRI has not yet been routinely used in the clinic, a few clinical studies have reported the potential applications of 4D-MRI in adaptive radiotherapy, online treatment guidance, and MRI-only workflow. For example, in adaptive radiotherapy, the radiotherapy plans could be adapted based on the registration position shifts between 4D-MRI and mid-position planning.⁴⁷ In the first clinical trial for abdominal stereotactic body radiation therapy (SBRT) with 4D-MRI-based online adaptation and real-time MRI monitoring, 10 patients were treated without the aid of CT.⁴⁸ As for online treatment guidance, multiple methods have been proposed for real-time volumetric cine-MRI.

For example, Harris et al. used principal component analysis (PCA) to model patients' breathing patterns and deformed prior images based on onboard 2D images to obtain 4D-MRI.^{49–51} The limitation of image processing speed impedes the clinical application of 4D-MRI in a real-time approach. Recently, the rapid development of artificial intelligence (AI) is expected to perform image processing tasks such as superposition, registration, and segmentation more efficiently and precisely, which may widen the clinical application of 4D-MRI.⁵² For example, Figure 6 demonstrates synthetic ultra-quality 4D-MRIs from the original 4D-MR image.

6 | MRI-BASED RADIOMICS MODELING

MRI has been widely used in quantitative modeling for radiotherapy assessments, such as diagnosis, prognosis, and toxicity predictions. Successful applications of MRI-based clinical modeling in radiotherapy could allow fully personalized treatment and follow-up strategies guided by MRI. Radiomics is one of the most popular quantitative approaches to analyzing medical images. It leverages the high-throughput features (e.g., size/shape-based features, intensity-based features, textural-based features) extracted from medical images using either predefined mathematical formulas or intermediate layers from deep-learning images.⁵³ Due to the higher soft-tissue contrast of MRI scans, MRI-based radiomics models have been demonstrated to sustain higher sensitivity to various clinical questions compared to other imaging modalities, making MRI a better candidate for tissue characterization. For example, the areas-under-curve (AUCs) of the MRI-based radiomics models were higher than those of CT-based models in both training and validation for radiation-induced xerostomia predictions 3 months after head-and-neck cancer radiotherapy.⁵⁴

Due to the availability of MRI scans at multiple time points of MRI-guided radiotherapy, the changes of MR radiomics feature in time, namely, delta-radiomics, can be monitored throughout the treatment course.⁵⁵ Delta radiomics has been proposed to predict final treatment responses so that the treatment plans can be adjusted between fractions at an individual level to achieve the optimized treatment outcome. One pilot study investigated the predictive power of

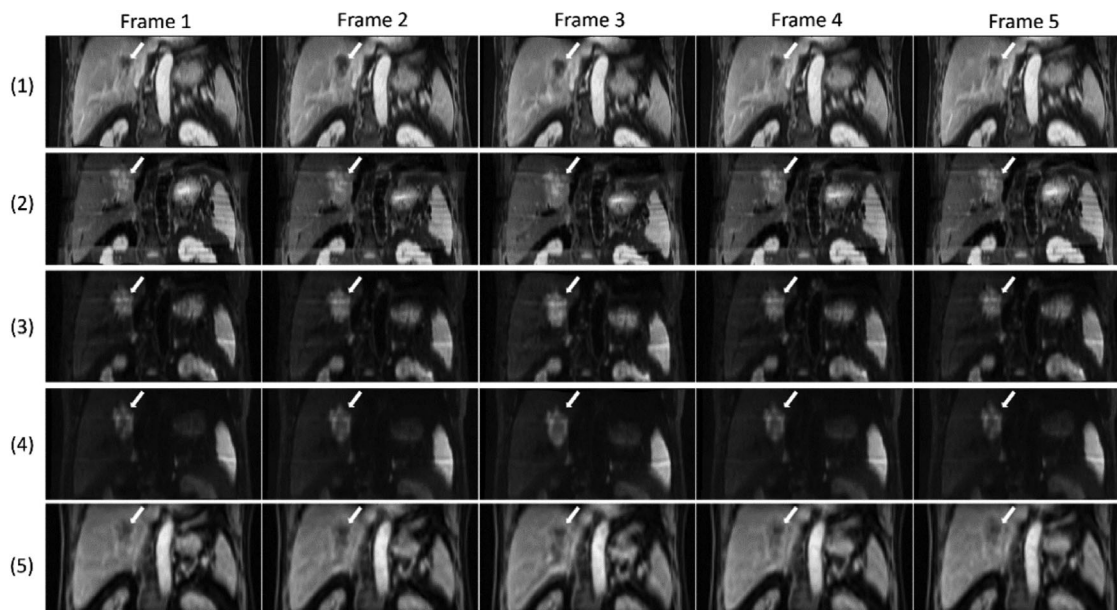


FIGURE 6 Visual examples of synthetic ultra-quality 4D-MRIs and the original T1w 4D-MRI. Tumors are indicated with arrows: (1) synthetic T1w 4D-MRI; (2) synthetic T2w 4D-MRI; (3) synthetic 4D-DWI ($b = 50$); (4) synthetic 4D-DWI ($b = 800$); (5) original T1w 4D-MRI

delta-radiomics on 16 rectal cancer patients undergoing magnetic MRI-guided radiotherapy. Radiomics features were extracted within GTV from six MRI scans on different treatment times, including the first MRI simulation and at fractions of 5, 10, 15, 20, and 25. Significant associations between multiple delta-radiomics features and complete clinical response were observed, indicating the promising future of personalized treatment surveillance in MRI-guided radiotherapy.⁵⁶ In another study, delta radiomics between the pretreatment and post-treatment MR images was used to predict 2-year distant metastasis locally advanced rectal cancer patients, and satisfactory performance of balanced accuracy of 78.5% was achieved on testing.⁵⁷

In addition to prognosis, MRI-based radiomics has been widely applied in diagnosis and toxicity predictions. A substudy following the prospective phase II trial on ultra-hypofractionated radiotherapy (AIRC IG-13218) has revealed multiple predictive MRI-based radiomics on diagnostic scores, including risk class, T-stage, Gleason score (GS), extracapsular extension (ECE) score, and Prostate Imaging Reporting and Data System (PI-RADS v2) score, which describe tumor aggressiveness for localized prostate cancer.⁵⁸ The areas under the receiver operating characteristic curve (ROC AUCs) remained high, with a range from 0.74 to 0.94. Hou et al. have developed a ready-to-use radiomics nomogram model that combines radiomics signatures from the T2-w MR images at the end of the radiotherapy and conventional clinical factors for radiotherapy-induced temporal lobe injury predictions of nasopharyngeal carcinoma patients.⁵⁹ The combined model has shown superior performance ($AUC = 0.87$) compared with single models that use only radiomics features and clinical features. Some studies have attempted to apply MR-based radiomics in clinical decision support such as adaptive radiotherapy. This is directly determined by the significant changes of patient anatomy, which is a wholistic effect from both tumor and normal tissue responses to radiation. For

example, Yu et al. have shown promising performances ($AUC = 0.984$ in training and 0.930 in testing) of combined radiomics features extracted from contrast-enhanced T1-weighted and T2-weighted MR images for adaptive radiotherapy eligibility predictions on advanced nasopharyngeal carcinoma patients.⁶⁰

Despite the promising future of radiomics in clinical modeling of MR-guided radiotherapy, the poor repeatability and reproducibility of many radiomics features have raised the concern of reliable clinical utilities. For instance, less than 10% of the total (1023) extracted radiomics features exhibit excellent repeatability between two MR-Linac scans, and they showed worse reproducibility between different MR scanners.⁶¹ Such high susceptibility of radiomics features to random and nonrandom variations imposes great challenges in routine clinical applications of radiomics-based models. Rigorous feature selection procedures that eliminate the low-robust features and detailed reporting of the image acquisition protocols and feature extraction parameters are of paramount importance in future developments of MRI radiomics clinical modeling in radiotherapy.

7 | MAGNETIC RESONANCE FINGERPRINTING

Magnetic resonance fingerprinting (MRF) is a novel MRI technique that achieves simultaneous tissue properties quantification within a single scan sequence.⁶² MRF employs a fast pulse sequence train with a series of pseudo-random flip angles (FA) and repetition times (TR) to generate highly under-sampled image sets. Every frame, or dynamic, in the image set has distinct contrast. As a result, each voxel formulates a signal evolution in the time domain. The signal evolution or “fingerprint” is unique for a specific tissue type. In addition to MRF scanning, the signal evolution could be simulated by the Bloch equation with parameters of

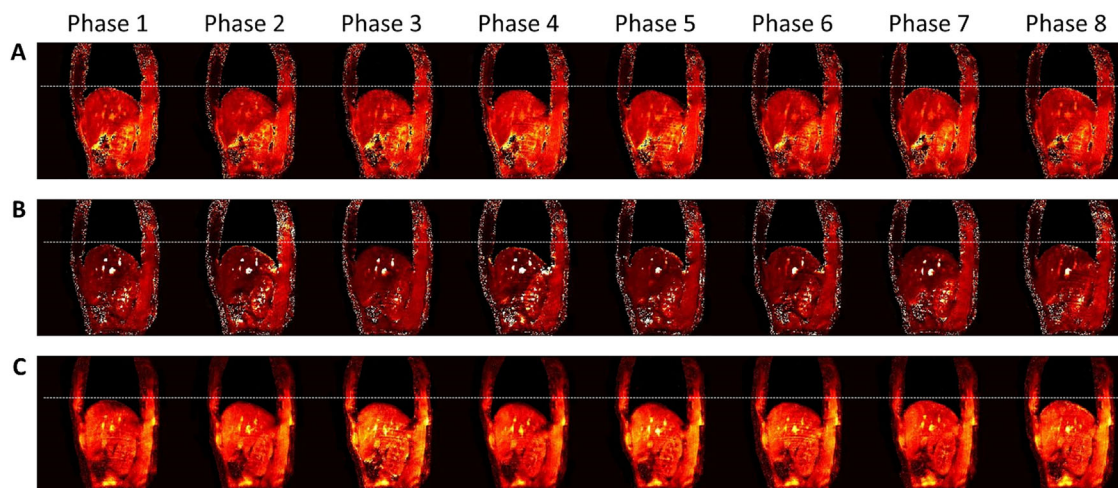


FIGURE 7 Tissue maps from multiple respiratory phases: A, T1 relaxation time map; B, T2 relaxation time map; C, proton density map

scanning protocols (e.g., FAs, TRs, time to echo [TE]) and tissue properties (e.g., T1 and T2 relaxation times, proton density). A dictionary that contains various tissue types is constructed by simulating a series of signal evolutions. By comparing with the signal evolutions acquired from the MRF scan with the dictionary, the tissue properties (e.g., T1 and T2 relaxation times, proton density) at each voxel could be retrieved.

MRF has great potential to improve MRI-guided radiotherapy workflow.⁶³ Contrary to conventional qualitative MRI scan schemes, the quantitative tissue maps derived from MRF demonstrated high repeatability and reproducibility.⁶⁴ These tissue maps may improve the accuracy of many MRI-related studies, such as CT synthesis and radiomics-based decision-making. The application of MRF to IGRT is promising. Simultaneous multi-parametric acquisition eliminates the uncertainty of image registration. Quantitative MRF biomarkers could be a reliable indicator for outcome prediction. One study has implemented MRF on MR-Linac, in which daily tissue maps are obtained.⁶⁵ In addition, the signal evolution could be retrospectively sorted for motion management.^{66,67} As shown in Figure 7, tissue maps from multiple phases could be obtained by re-binning and optimizing the MRF signal. Though promising, the development of the MRF technique is still in its early stages. This limitation still exists that impedes its clinical implementation and validation. First, to date, the MRF scan sequence is not clinically available. Second, the MRF scan time is prohibitive longer than the commercial sequence. For example, the acquisition time for a 2D slice is about 10s and 10 min for a 3D volume. Lastly, the reconstruction is time-consuming and computational power demanding. These limitations impede the clinical implementation and validation of MRF.

8 | CONCLUSION

This paper reviews recent technical advances in MRI-guided precision radiotherapy. The rapid development of MR imaging and image pro-

cessing techniques have substantially improved the performance and expanded the capacity of MRI-guided radiotherapy. With the assistance of AI and data science, MRI-guided radiotherapy is moving toward to real-time and online adaptive, contributing to the personalized precision radiotherapy.

ACKNOWLEDGMENTS

This research was partly supported by research grants of the General Research Fund (GRF 15102118, GRF 15102219), the University Grants Committee, Health and Medical Research Fund (HMRF 06173276), the Food and Health Bureau, and the Innovation and Technology Fund (ITS/080/19), the Innovation and Technology Commission, the Government of the Hong Kong Special Administrative Region.

CONFLICT OF INTEREST

Mao Li is an employee of Philips Healthcare. Other authors declare no competing interests.

ORCID

Jing Cai  <https://orcid.org/0000-0001-6934-0108>

REFERENCES

1. Baskar R, Lee KA, Yeo R, Yeoh KW. Cancer and radiation therapy: current advances and future directions. *Int J Med Sci.* 2012;9(3):193–199.
2. Yu J, Xing L. Precision radiation oncology: achievements and challenges. *Precis Radiat Oncol.* 2017;1(1):4–6.
3. Dawson LA, Jaffray DA. Advances in image-guided radiation therapy. *J Clin Oncol.* 2007;25(8):938–946. <https://doi.org/10.1200/JCO.2006.09.9515>
4. Gupta T, Beriwal S. PET/CT-guided radiation therapy planning: from present to the future. *Indian J Cancer.* 2010;47(2):126–133.
5. Tyagi N, Zelefsky MJ, Wibmer A, et al. Clinical experience and workflow challenges with magnetic resonance-only radiation therapy simulation and planning for prostate cancer. *Phys Imaging Radiat Oncol.* 2020; 16: 43–49.
6. Chin S, Eccles CL, McWilliam A, et al. Magnetic resonance-guided radiation therapy: a review. *J Med Imaging Radiat Oncol.* 2020;64(1):163–177.

7. Siddique S, Chow JCL. Artificial intelligence in radiotherapy. *Rep Pract Oncol Radiother*. 2020;25(4):656–666.
8. Dimopoulos JC, Petrow P, Tanderup K, et al. Recommendations from gynaecological (GYN) GEC-ESTRO working group (IV): basic principles and parameters for MR imaging within the frame of image based adaptive cervix cancer brachytherapy. *Radiother Oncol*. 2012;103(1):113–122.
9. Wang J, Tanderup K, Cunha A, et al. Magnetic resonance imaging basics for the prostate brachytherapist. *Brachytherapy*. 2017;16(4):715–727.
10. Okamoto Y, Imanaka K, Sakaguchi T, et al. Fundamental study on development of MRI simulation system for radiotherapy planning. *Int J Radiat Oncol Biol Phys*. 1993;27:303. [https://doi.org/10.1016/0360-3016\(93\)90917-K](https://doi.org/10.1016/0360-3016(93)90917-K)
11. Schubert K, Wenz F, Krempien R, et al. Einsatzmöglichkeiten eines offenen magnetresonanztomographen in der therapiesimulation und dreidimensionalen bestrahlungsplanung [Possibilities of an open magnetic resonance scanner integration in therapy simulation and three-dimensional radiotherapy planning. *Strahlenther Onkol*. 1999;175(5):225–231.
12. Paulson ES, Crijns SP, Keller BM, et al. Consensus opinion on MRI simulation for external beam radiation treatment planning. *Radiother Oncol*. 2016;121(2):187–192.
13. Hua CH, Uh J, Krasin MJ, et al. Clinical implementation of magnetic resonance imaging systems for simulation and planning of pediatric radiation therapy. *J Med Imaging Radiat Sci*. 2018;49(2):153–163.
14. Bainbridge H, Salem A, Tijssen RHN, et al. Magnetic resonance imaging in precision radiation therapy for lung cancer. *Transl Lung Cancer Res*. 2017;6(6):689–707.
15. Ligtenberg H, Schakel T, Dankbaar JW, et al. Target volume delineation using diffusion-weighted imaging for MR-guided radiotherapy: a case series of laryngeal cancer validated by pathology. *Cureus*. 2018;10(4):e2465. <https://doi.org/10.7759/cureus.2465>
16. Liney GP, Whelan B, Oborn B, Barton M, Keall P. MRI-linear accelerator radiotherapy systems. *Clin Oncol (R Coll Radiol)*. 2018;30(11):686–691.
17. Raaymakers BW, Jürgenliemk-Schulz IM, Bol GH, et al. First patients treated with a 1.5 T MRI-Linac: clinical proof of concept of a high-precision, high-field MRI guided radiotherapy treatment. *Phys Med Biol*. 2017;62(23):L41–L50.
18. Winkel D, Bol GH, Kroon PS, et al. Adaptive radiotherapy: the Elekta unity MR-linac concept. *Clin Transl Radiat Oncol*. 2019;18:54–59.
19. Kontaxis C, de Muinck Keizer DM, Kerkmeijer LGW, et al. Delivered dose quantification in prostate radiotherapy using online 3D cine imaging and treatment log files on a combined 1.5T magnetic resonance imaging and linear accelerator system. *Phys Imaging Radiat Oncol*. 2020;15:23–29.
20. Borman PTS, Tijssen RHN, Bos C, Moonen CTW, Raaymakers BW, Glitzner M. Characterization of imaging latency for real-time MRI-guided radiotherapy. *Phys Med Biol*. 2018;63(15):155023. <https://doi.org/10.1088/1361-6560/aad2b7>
21. Kontaxis C, Bol GH, Lagendijk JJW, Raaymakers BW. DeepDose: towards a fast dose calculation engine for radiation therapy using deep learning. *Phys Med Biol*. 2020;65(7):075013. <https://doi.org/10.1088/1361-6560/ab7630>
22. Li W, Li Y, Qin W, et al. Magnetic resonance image (MRI) synthesis from brain computed tomography (CT) images based on deep learning methods for magnetic resonance (MR)-guided radiotherapy. *Quant Imaging Med Surg*. 2020;10(6):1223–1236.
23. Song L, Li Y, Dong G, et al. Artificial intelligence-based bone-enhanced magnetic resonance image—a computed tomography/magnetic resonance image composite image modality in nasopharyngeal carcinoma radiotherapy. *Quant Imaging Med Surg*. 2021;11(12):4709–4720.
24. Edmund JM, Nyholm T. A review of substitute CT generation for MRI-only radiation therapy. *Radiat Oncol*. 2017;12(1):28. <https://doi.org/10.1186/s13014-016-0747-y>
25. Bratova I, Paluska P, Grepl J, et al. Validation of dose distribution computation on sCT images generated from MRI scans by Philips MRCAT. *Rep Pract Oncol Radiother*. 2019;24(2):245–250.
26. Li W, Kazemifar S, Bai T, et al. Synthesizing CT images from MR images with deep learning: model generalization for different datasets through transfer learning. *Biomed Phys Eng Express*. 2021;7(2):025020. <https://doi.org/10.1088/2057-1976/abe3a7>
27. Glover GH. Overview of functional magnetic resonance imaging. *Neurosurg Clin N Am*. 2011;22(2):133–vii. <https://doi.org/10.1016/j.nec.2010.11.001>
28. Olsson LE, Johansson M, Zackrisson B, Blomqvist LK. Basic concepts and applications of functional magnetic resonance imaging for radiotherapy of prostate cancer. *Phys Imaging Radiat Oncol*. 2019;9:50–57.
29. Hu L, Zhou DW, Zha YF, et al. Synthesizing high-b-value diffusion-weighted imaging of the prostate using generative adversarial networks. *Radiol Artif Intell*. 2021;3(5):e200237. <https://doi.org/10.1148/ryai.2021200237>
30. Sieber MA, Steger-Hartmann T, Lengsfeld P, Pietsch H. Gadolinium-based contrast agents and NSF: evidence from animal experience. *J Magn Reson Imaging*. 2009;30(6):1268–1276.
31. Zhang B, Liang L, Chen W, Liang C, Zhang S. An updated study to determine association between gadolinium-based contrast agents and nephrogenic systemic fibrosis. *PLoS One*. 2015;10(6):e0129720. <https://doi.org/10.1371/journal.pone.0129720>
32. Ramalho J, Semelka RC, Ramalho M, Nunes RH, Alobaidy M, Castillo M. Gadolinium-based contrast agent accumulation and toxicity: an update. *AJNR Am J Neuroradiol*. 2016;37(7):1192–1198.
33. Gong E, Pauly JM, Wintermark M, Zaharchuk G. Deep learning enables reduced gadolinium dose for contrast-enhanced brain MRI. *J Magn Reson Imaging*. 2018;48(2):330–340.
34. Kleesiek J, Morshuis JN, Isensee F, et al. Can virtual contrast enhancement in brain MRI replace gadolinium? A feasibility study. *Invest Radiol*. 2019;54(10):653–660.
35. Chen C, Raymond C, Speier B, et al. Synthesizing MR image contrast enhancement using 3D high-resolution ConvNets. *ArXiv*. 2021. [abs/2104.01592](https://arxiv.org/abs/2104.01592).
36. Cai J, Read PW, Altes TA, Molloy JA, Brookeman JR, Sheng K. Evaluation of the reproducibility of lung motion probability distribution function (PDF) using dynamic MRI. *Phys Med Biol*. 2007;52(2):365–373.
37. Cai J, Read PW, Larner JM, Jones DR, Benedict SH, Sheng K. Reproducibility of interfraction lung motion probability distribution function using dynamic MRI: statistical analysis. *Int J Radiat Oncol Biol Phys*. 2008;72(4):1228–1235.
38. Stemkens B, Paulson ES, Tijssen RHN. Nuts and bolts of 4D-MRI for radiotherapy. *Phys Med Biol*. 2018;63(21):21TR01. <https://doi.org/10.1088/1361-6560/aee56d>
39. Liu Y, Zhong X, Czito BG, et al. Four-dimensional diffusion-weighted MR imaging (4D-DWI): a feasibility study. *Med Phys*. 2017;44(2):397–406.
40. Liu Y, Yin FF, Czito BG, Bashir MR, Cai J. T2-weighted four dimensional magnetic resonance imaging with result-driven phase sorting. *Med Phys*. 2015;42(8):4460–4471.
41. Yang J, Cai J, Wang H, et al. Is diaphragm motion a good surrogate for liver tumor motion? *Int J Radiat Oncol Biol Phys*. 2014;90(4):952–958.
42. Keijnevans K, Borman PTS, van Lier A LHMW, Verhoeff JJC, Raaymakers BW, Fast MF. Simultaneous multi-slice accelerated 4D-MRI for radiotherapy guidance. *Phys Med Biol*. 2021;66(9):095014. <https://doi.org/10.1088/1361-6560/abf591>
43. Navest RJM, Mandija S, Bruijnen T, et al. The noise navigator: a surrogate for respiratory-correlated 4D-MRI for motion characterization in radiotherapy. *Phys Med Biol*. 2020;65(1):01NT02. <https://doi.org/10.1088/1361-6560/ab5c62>
44. Yang J, Cai J, Wang H, et al. Four-dimensional magnetic resonance imaging using axial body area as respiratory surrogate: initial patient results. *Int J Radiat Oncol Biol Phys*. 2014;88(4):907–912.

45. Li G, Wei J, Olek D, et al. Direct comparison of respiration-correlated four-dimensional magnetic resonance imaging reconstructed using concurrent internal navigator and external bellows. *Int J Radiat Oncol Biol Phys*. 2017;97(3):596–605.
46. Yuan J, Wong OL, Zhou Y, Chueng KY, Yu SK. A fast volumetric 4D-MRI with sub-second frame rate for abdominal motion monitoring and characterization in MRI-guided radiotherapy. *Quant Imaging Med Surg*. 2019;9(7):1303–1314.
47. van de Lindt TN, Fast MF, van den Wollenberg W, et al. Validation of a 4D-MRI guided liver stereotactic body radiation therapy strategy for implementation on the MR-linac. *Phys Med Biol*. 2021;66(10):105010. [10.1088/1361-6560/abfada](https://doi.org/10.1088/1361-6560/abfada)
48. Hall WA, Straza MW, Chen X, et al. Initial clinical experience of stereotactic body radiation therapy (SBRT) for liver metastases, primary liver malignancy, and pancreatic cancer with 4D-MRI based online adaptation and real-time MRI monitoring using a 1.5 T MR-Linac [published correction appears in PLoS One. 2020 Nov 4;15(11):e0242146]. *PLoS One*. 2020;15(8):e0236570. <https://doi.org/10.1371/journal.pone.0236570>. Published Aug 7, 2020.
49. Harris W, Yin FF, Cai J, Ren L. Volumetric cine magnetic resonance imaging (VC-MRI) using motion modeling, free-form deformation and multi-slice undersampled 2D cine MRI reconstructed with spatio-temporal low-rank decomposition. *Quant Imaging Med Surg*. 2020;10(2):432–450.
50. Harris W, Wang C, Yin FF, Cai J, Ren L. A novel method to generate on-board 4D MRI using prior 4D MRI and on-board kV projections from a conventional LINAC for target localization in liver SBRT. *Med Phys*. 2018;45(7):3238–3245.
51. Harris W, Ren L, Cai J, Zhang Y, Chang Z, Yin FF. A technique for generating volumetric cine-magnetic resonance imaging. *Int J Radiat Oncol Biol Phys*. 2016;95(2):844–853.
52. Xiao H, Teng X, Liu C, et al. A review of deep learning-based three-dimensional medical image registration methods. *Quant Imaging Med Surg*. 2021;11(12):4895–4916.
53. van Timmeren JE, Cester D, Tanadini-Lang S, Alkadhi H, Baessler B. Radiomics in medical imaging—“how-to” guide and critical reflection. *Insights Imaging*. 2020;11(1):91. <https://doi.org/10.1186/s13244-020-00887-2>
54. Sheikh K, Lee SH, Cheng Z, et al. Predicting acute radiation induced xerostomia in head and neck cancer using MR and CT radiomics of parotid and submandibular glands. *Radiat Oncol*. 2019;14(1):131. <https://doi.org/10.1186/s13014-019-1339-4>
55. Jeon SH, Song C, Chie EK, et al. Delta-radiomics signature predicts treatment outcomes after preoperative chemoradiotherapy and surgery in rectal cancer. *Radiat Oncol*. 2019;14(1):43. <https://doi.org/10.1186/s13014-019-1246-8>
56. Boldrini L, Cusumano D, Chiloiro G, et al. Delta radiomics for rectal cancer response prediction with hybrid 0.35 T magnetic resonance-guided radiotherapy (MRgRT): a hypothesis-generating study for an innovative personalized medicine approach. *Radiol Med*. 2019;124(2):145–153.
57. Chiloiro G, Rodriguez-Carnero P, Lenkovicz J, et al. Delta radiomics can predict distant metastasis in locally advanced rectal cancer: the challenge to personalize the cure. *Front Oncol*. 2020;10:595012. <https://doi.org/10.3389/fonc.2020.595012>
58. Gugliandolo SG, Pepa M, Isaksson LJ, et al. MRI-based radiomics signature for localized prostate cancer: a new clinical tool for cancer aggressiveness prediction? Sub-study of prospective phase II trial on ultra-hypofractionated radiotherapy (AIRC IG-13218). *Eur Radiol*. 2021;31(2):716–728.
59. Hou J, Li H, Zeng B, et al. MRI-based radiomics nomogram for predicting temporal lobe injury after radiotherapy in nasopharyngeal carcinoma [published online ahead of print, Aug 31, 2021]. *Eur Radiol*. 2021. [https://doi.org/10.1007/s00330-021-08254-5\(2021\)](https://doi.org/10.1007/s00330-021-08254-5(2021))
60. Yu TT, Lam SK, To LH, et al. pretreatment prediction of adaptive radiation therapy eligibility using MRI-based radiomics for advanced nasopharyngeal carcinoma patients. *Front Oncol*. 2019;9:1050. <https://doi.org/10.3389/fonc.2019.01050>
61. Xue C, Yuan J, Poon DM, et al. Reliability of MRI radiomics features in MR-guided radiotherapy for prostate cancer: repeatability, reproducibility, and within-subject agreement. *Med Phys*. 2021;48(11):6976–6986.
62. Ma D, Gulani V, Seiberlich N, et al. Magnetic resonance fingerprinting. *Nature*. 2013;495(7440):187–192.
63. Lu L, Chen Y, Shen C, et al. Initial assessment of 3D magnetic resonance fingerprinting (MRF) towards quantitative brain imaging for radiation therapy. *Med Phys*. 2020;47(3):1199–1214.
64. Panda A, Chen Y, Ropella-Panagis K, et al. Repeatability and reproducibility of 3D MR fingerprinting relaxometry measurements in normal breast tissue. *J Magn Reson Imaging*. 2019;50(4):1133–1143.
65. Bruijnen T, van der Heide O, Intven MPW, et al. Technical feasibility of magnetic resonance fingerprinting on a 1.5 T MRI-linac. *Phys Med Biol*. 2020;65(22):22NT01. <https://doi.org/10.1088/1361-6560/abbb9d>
66. Li T, Cui D, Hui ES, Cai J. Time-resolved magnetic resonance fingerprinting for radiotherapy motion management [published correction appears in Med Phys. 2021 May;48(5):2698]. *Med Phys*. 2020;47(12):6286–6293.
67. Li T, Cui D, Ren G, Hui ES, Cai J. Investigation of the effect of acquisition schemes on time-resolved magnetic resonance fingerprinting. *Phys Med Biol*. 2021;66(9). [10.1088/1361-6560/abf51f](https://doi.org/10.1088/1361-6560/abf51f)

How to cite this article: Liu C, Li M, Xiao H, et al. Advances in MRI-guided precision radiotherapy. *Prec Radiat Oncol*. 2022;6:75–84. <https://doi.org/10.1002/pro6.1143>